International Journal of Bifurcation and Chaos, Vol. 22, No. 6 (2012) 1230021 (15 pages)

DOI: 10.1142/S0218127412300212

NUMERICAL ANALYSIS OF TRANSIENT AND PERIODIC DYNAMICS IN SINGLE AND COUPLED NAGUMO–SATO MODELS

MAKITO OKU* and KAZUYUKI AIHARA
Institute of Industrial Science, The University of Tokyo,
4-6-1 Komaba, Meguro-ku, Tokyo 153-8505, Japan
**oku@sat.t.u-tokyo.ac.jp*

Received February 8, 2012

The Nagumo–Sato (NS) model is a one-dimensional piecewise linear map that describes simplified dynamics of a single neuron. The NS model and its network extension, coupled Nagumo–Sato models, exhibit complex behavior both in their transient dynamics and after converging to periodic orbits. However, the way the period and the transient length change against the parameters is not completely understood. In this study, we numerically investigate the transient and periodic dynamics in single and coupled NS models. Simulation results indicate the following observations. (1) The period of a single NS model shows layered structures associated with the Farey sequence. (2) Two coupled NS models show discontinuity in the transient length, even though the period does not change. (3) In the case of an associative memory model consisting of NS models, there exists a small parameter region where both the period and the transient length increase considerably. The dynamics within the region is much more complex than that outside the region.

Keywords: Nagumo–Sato model; piecewise linear map; devil's staircase; Farey sequence; transient dynamics.

1. Introduction

The Nagumo–Sato (NS) model [Nagumo & Sato, 1972] is a one-dimensional piecewise linear map described as

$$x(t+1) = F(x(t)) = k\,x(t) - u(x(t)) + a, \quad (1)$$

where $x \in \mathbb{R}$ is the state variable, t with $t = 0, 1, 2, \ldots$ is the time step, $k \in [0, 1)$ and $a \in [0, 1]$ are the parameters, and u is the step function, i.e. $u(x) = 1$ for $x \geq 0$ and $u(x) = 0$ for $x < 0$. Hence, Eq. (1) can be rewritten as

$$x(t+1) = \begin{cases} kx(t) - 1 + a & \text{if } x \geq 0, \\ kx(t) + a & \text{if } x < 0. \end{cases} \quad (2)$$

As can be seen from the above equation, the map includes discontinuity at $x = 0$. This type of dynamical system is called a hybrid dynamical system [Aihara & Suzuki, 2010], in which both the continuous and discrete dynamics coexist. The typical behavior of the model is illustrated in Fig. 1.

The NS model describes simplified dynamics of a single neuron, including the threshold mechanism and the refractoriness effect of the neuron. The model can also reproduce complicated stepwise response of an artificial neuron model implemented in an electrical circuit [Harmon, 1961]. This stepwise response is known as the devil's staircase [Bak, 1986].

The NS model corresponds to a special case of Caianiello's model [Caianiello, 1961]. Caianiello's model allows an arbitrary form of the influence of previous firing events on the current state variable. On the other hand, the NS model assumes that the refractoriness effect decays exponentially. Another generalization of the NS model is the chaotic neuron

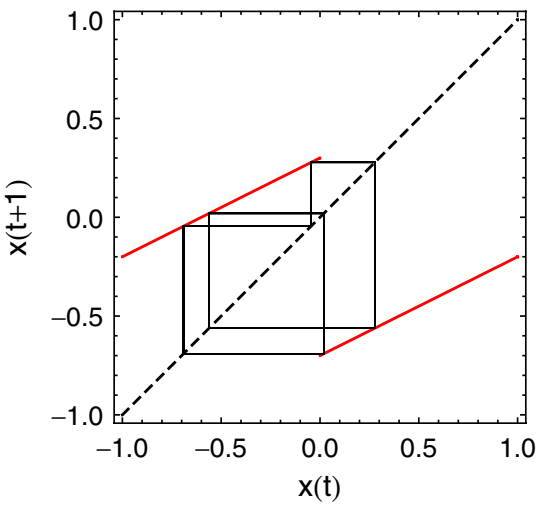

Fig. 1. Typical behavior of the Nagumo–Sato model. Two red lines show the map $x(t+1) = F(x(t))$. The diagonal dashed line is the identity map, which is shown for reference. Solid black lines show the orbit of a stable period-5 solution with $a = 0.3$ and $k = 0.5$.

model [Aihara, 1990; Aihara *et al.*, 1990], in which a sigmoid function substitutes for the step function in Eq. (1). Similarly, networks of the NS models are also generalized [Aihara, 1990; Aihara *et al.*, 1990]. The NS model also describes various phenomena such as the Belousov–Zhabotinsky reaction [Tomita & Tsuda, 1980; Tsuda, 1981] and the on-off sampled-data control [Bockman, 1991]. Furthermore, the model was rediscovered as a variant of the circle map [Ding & Hemmer, 1987]. For more details on the relationship between the NS model and other mathematical models, see [Aihara & Suzuki, 2010].

The state variable of the NS model does not diverge to infinity because within the abovementioned parameter range, every trajectory eventually falls in the interval $[a-1, a]$. In addition, the model does not exhibit chaotic behavior. Indeed, the Lyapunov exponent of the NS model is

$$\lambda = \lim_{T\to\infty} \frac{1}{T} \sum_{t=0}^{T-1} \ln \left| \frac{\mathrm{d}F(x(t))}{\mathrm{d}x(t)} \right| = \ln k < 0. \quad (3)$$

Thus, the model does not show orbital instability in terms of a positive Lyapunov exponent.

The NS model has a unique attractor for each realization of the parameters a and k. In almost all cases, the attractor is periodic; nonperiodic attractors exist only for a parameter set that has zero Lebesgue measure in the parameter space [Nagumo & Sato, 1972; Hata, 1982, 1998; Ding & Hemmer, 1987]. Thus, almost all the trajectories observable in numerical simulations are either stable periodic orbits or their transient dynamics. Note that the nonperiodic solutions have some characteristics that are mathematically interesting. First, the parameters corresponding to the nonperiodic attractors form a self-similar Cantor set. Next, each trajectory of the nonperiodic attractors has an invariant set that corresponds to a Cantor set in the state space. Moreover, the nonperiodic attractors gain a type of orbital instability [Hata, 1982, 1998], which is different from typical orbital instability that is based on an exponential growth of perturbations. Although these nonperiodic attractors are numerically intractable, they may contribute to the complexity of observable trajectories as their background structures.

The network extension of the NS model, coupled NS models, can be described as

$$x_i(t+1) = k\, x_i(t) - y_i(t) + a, \quad (4)$$

$$y_i(t+1) = u\left(x_i(t+1) + \sum_{j=1}^{N} w_{ij} y_j(t) \right), \quad (5)$$

where x_i is the state variable of node i; $y_i \in \{0, 1\}$, the output of node i; w_{ij}, the connection weight from node j to node i; and N, the number of nodes. The weighted summation of the inputs from the other nodes is not directly added to the original one-dimensional map (1). Instead, it modulates the next output, as in Eq. (5). This network system is a special case of the chaotic neural network model [Adachi & Aihara, 1997] and has $2N$ degrees of freedom. The maximum Lyapunov exponent is negative for $k < 1$.

There is another type of coupled NS models, in which the analog values of x_i are directly transmitted via diffusive coupling [Crutchfield & Kaneko, 1988; Politi *et al.*, 1993; Kinoshita *et al.*, 2010]. This type of connections correspond to electrical synapses or gap junctions in biological neural networks. In contrast, the connections used in Eq. (5) correspond to chemical synapses. A notable feature of the electrical-synapse-type connections is that if a set of NS models is arranged in a regular lattice, which is called a coupled map lattice [Kaneko, 1985], the network exhibits very long transient dynamics before the system abruptly falls in a relatively short periodic solution [Crutchfield & Kaneko, 1988; Politi *et al.*, 1993]. This kind of long transient dynamics is called the type-II supertransient and has been widely investigated

[Kaneko, 1990]. In this study, however, we restrict ourselves to the chemical-synapse-type connections.

The single and coupled NS models exhibit complex behavior despite a negative maximum Lyapunov exponent. Such nonchaotic behavior corresponds to a stable periodic orbit and its transient dynamics, if the parameters and the initial states are general. However, the underlying mechanism of the complex behavior and the way the period and the transient length change against the parameters are not completely elucidated.

The definitions of the period and the transient length are as follows. Let $X(t)$ denote the system's state at time t. Note that in numerical simulations, the system can reach a periodic orbit within finite steps because the precision is finite. The transient length τ is defined as the minimum number that satisfies $\exists p' \in \mathbb{N},\ \forall t \geq \tau,\ X(t+p') = X(t)$. The period p is defined as the minimum number of p'. To calculate p and τ, we use an algorithm that is suitable for the cases of large p and τ (see Appendix).

In this study, we numerically investigate the period and the transient length in single and coupled NS models. In particular, we investigate: a single NS model (Sec. 2), two coupled NS models (Sec. 3), and an associative memory model consisting of NS models (Sec. 4). We present our conclusions in Sec. 5.

2. Single NS Model

The NS model shows a complicated stepwise increase in the firing rate ρ as the parameter a increases [Nagumo & Sato, 1972]. The firing rate is defined as

$$\rho = \lim_{T\to\infty} \frac{1}{T} \sum_{t=0}^{T-1} u(x(t)). \tag{6}$$

We assume that the initial state, $x(0)$, and the parameters, a and k, are in general positions so that the system converges to a stable periodic orbit. With this assumption, the firing rate becomes

$$\rho = \frac{1}{p} \sum_{r=1}^{p} u(x^r), \tag{7}$$

where $\{x^1, \ldots, x^p\}$ is a set of periodic points. The firing rate is also called the winding number [Ding & Hemmer, 1987]. In the case of coupled NS models, the firing rate is redefined as the mean value of each node's firing rate ρ_i $(i = 1, \ldots, N)$, i.e. $\rho = (1/N)\sum_{i=1}^{N} \rho_i$.

Figure 2(a) shows the phase diagram of the firing rate of a single NS model. The entire parameter space is divided by many subregions with distinct values of the firing rate. A similar structure is also observed in the phase diagram of the period, as shown in Fig. 2(b). This type of structure has also been obtained with different parameterizations of the NS model [Ding & Hemmer, 1987; Kinoshita *et al.*, 2010].

On the other hand, the phase diagram of the average transient length is considerably less structured, as shown in Fig. 2(c). Note that the transient length depends on the initial state $x(0)$. Thus, we consider the average values over different initial conditions. The average transient length increases with k, whereas the value of a produces little change in the average transient length. To reveal the delicate structure associated with a, we perform a thresholding operation on the phase diagram. Let $\tau_{a,k}$ denote the average transient length at parameter values a and k. Let $\tau_k = \langle \tau_{a,k} \rangle_a$ denote the average value of $\tau_{a,k}$ with respect to a. Then, the thresholded transient length is given by $\tilde{\tau}_{a,k} = u(\tau_{a,k} - \tau_k)$. In other words, we plot a point where the average transient length is relatively long. Figure 2(d) shows the phase diagram of the thresholded transient length $\tilde{\tau}_{a,k}$. We observe a structure similar to those in Figs. 2(a) and 2(b). In the numerical simulation for Fig. 2(d), we carefully use fixed-point numbers instead of floating-point numbers because the transient length is perturbed slightly by the adaptive scaling of the floating-point numbers, which induces some artifacts in the phase diagram. On the other hand, the other three phase diagrams, shown in Figs. 2(a)–2(c), are similar for both types of numbers.

If we fix k and increase a, the firing rate shows a devil's staircase pattern, as shown in Fig. 3(a). Similarly, if we fix a and increase k, another complicated staircase pattern can be observed, as shown in Fig. 3(b). On the other hand, the changes in the period and the transient length against each of the parameters are shown in Figs. 3(c) and 3(d). The transient length fluctuates around the mean value because of different initial states, and it is always larger than the period. The period does not increase monotonously against each parameter. Instead, it becomes large at short intervals of constant value against parameters, whereas it is small at longer

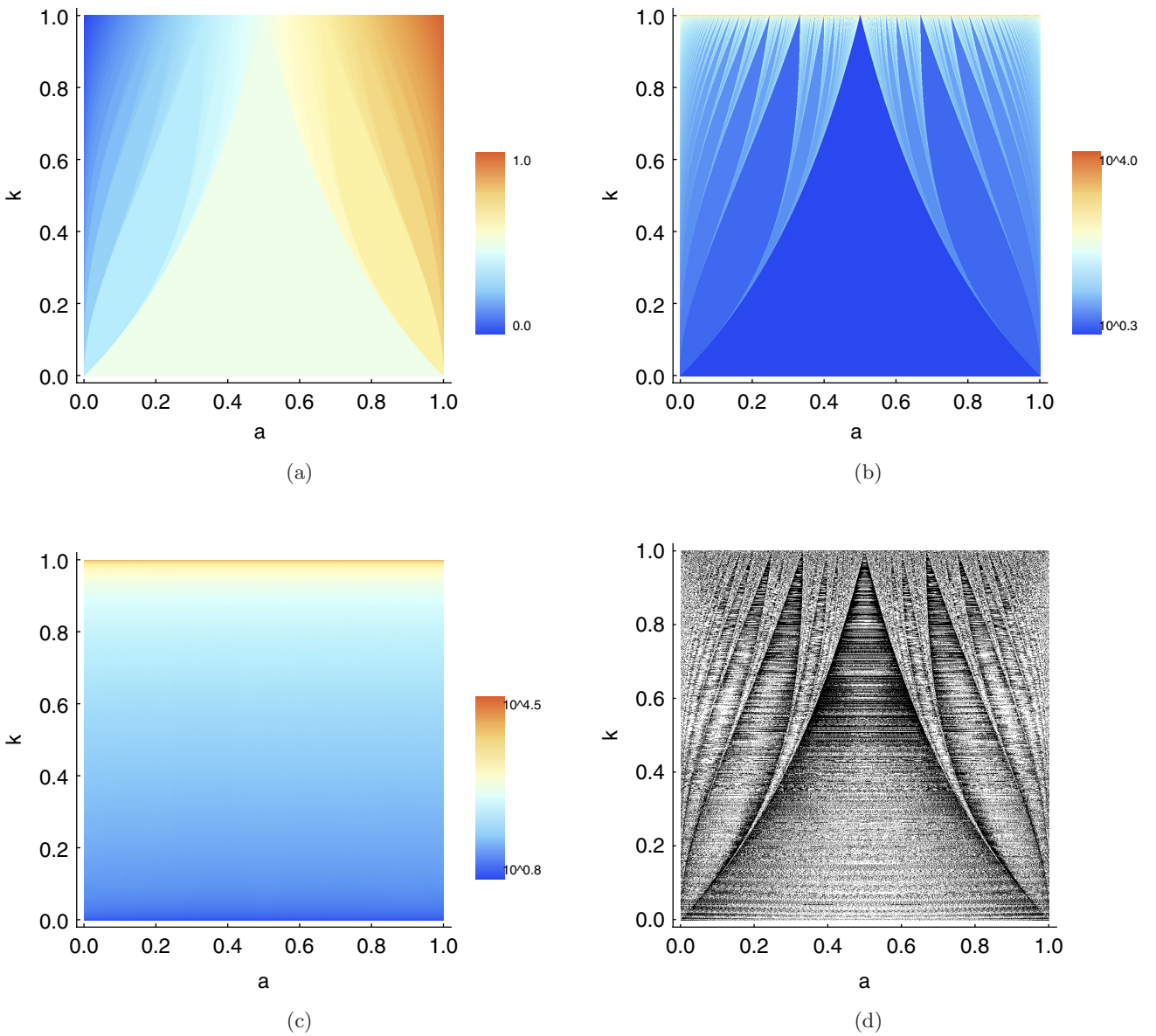

Fig. 2. Phase diagrams of a single Nagumo–Sato model. (a) Firing rate. (b) Period. (c) Average transient length. (d) Thresholded transient length. Both the parameters a and k are varied from 0.001 to 0.999. The color bars in (b) and (c) are scaled logarithmically. Plots (c) and (d) involve 101 trials of different initial states that are equally spaced within $[-1, 1]$. Plot (d) is calculated using fixed-point numbers, whereas the others are calculated using floating-point numbers.

intervals. Moreover, we can draw a few envelopes that link a part of the intervals. Accordingly, the intervals can be categorized into several groups, which yield layered structures. These layered structures can also be observed with other parameter settings. However, the layered structure with respect to the parameter k disappears at $a \simeq 0.4$ and $a \simeq 0.6$.

The period diverges as $a \to 0$ and $a \to 1$. Figure 3(e) shows an enlarged view for a close to 0, where the horizontal axis is scaled logarithmically. This plot indicates $p \propto -\ln a$ as $a \to 0$. Note that the stepwise function in Fig. 3(a) is symmetrical with respect to the point $(a, \rho) = (1/2, 1/2)$ because map (1) is invariant under the transformation with $a' = 1 - a$ and $x' = -x$. Thus, we obtain the relationship $p \propto -\ln(1-a)$ as $a \to 1$. On the other hand, the period diverges as $k \to 1$. Figure 3(f) shows a log–log plot for k close to 1. This plot indicates $p, \tau \propto 1/(1-k)$ as $k \to 1$. In addition, a layered structure is clearly seen in the period.

Figure 4 shows two layered structures for k close to 1. These layered structures are associated with

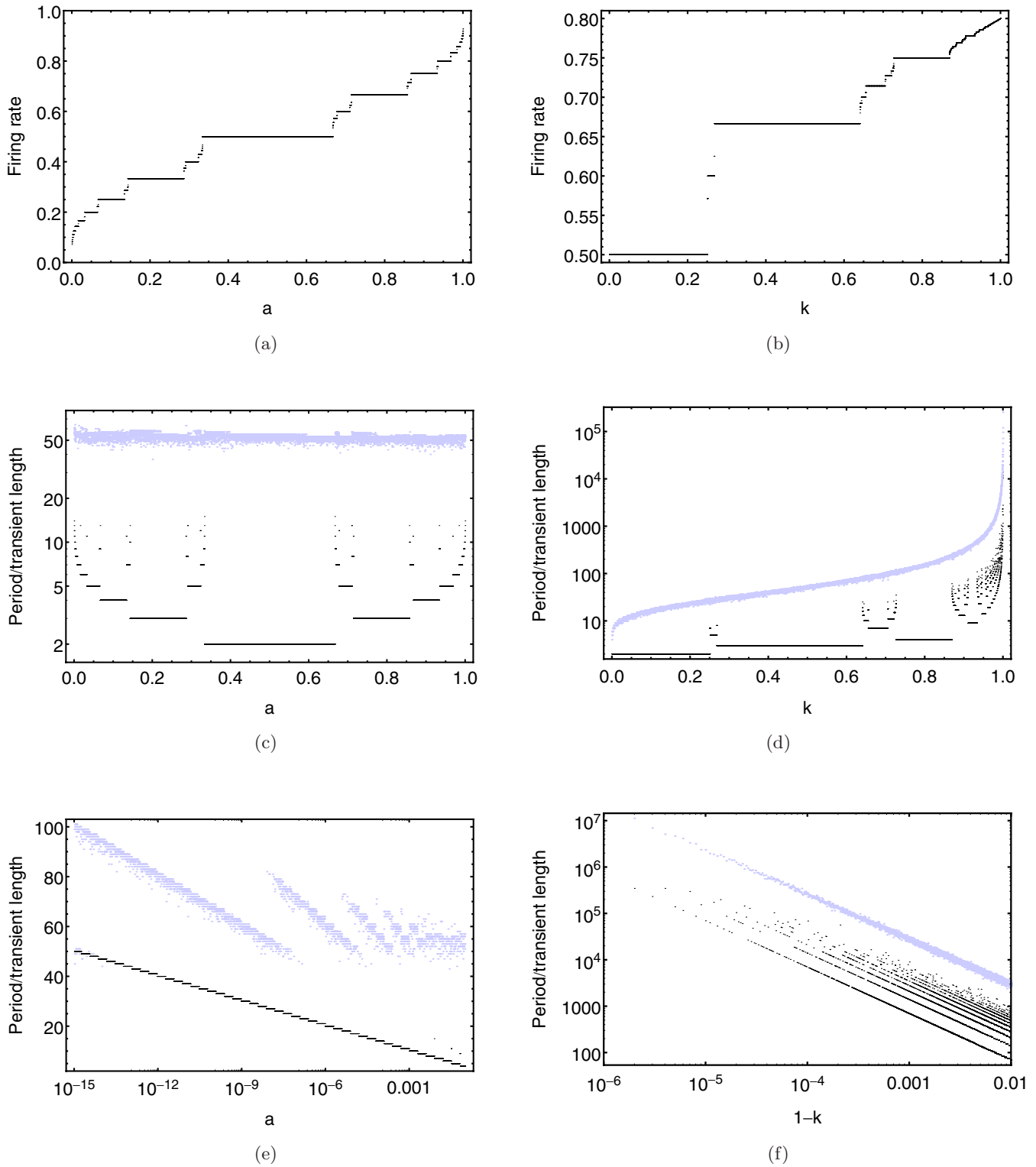

Fig. 3. (Top row) Devil's staircases with respect to (a) the parameter a and (b) the parameter k. (Middle row) Plots of the period and the transient length. (Bottom row) Enlarged views for (e) a close to 0 and (f) k close to 1. In (a), (c) and (e), we set $k = 0.5$. In (b), (d) and (f), we set $a = 0.8$. The black and blue dots in (c)–(f) show the period and the transient length, respectively. Initial states are randomly sampled from the uniform distribution in $[-1, 1]$.

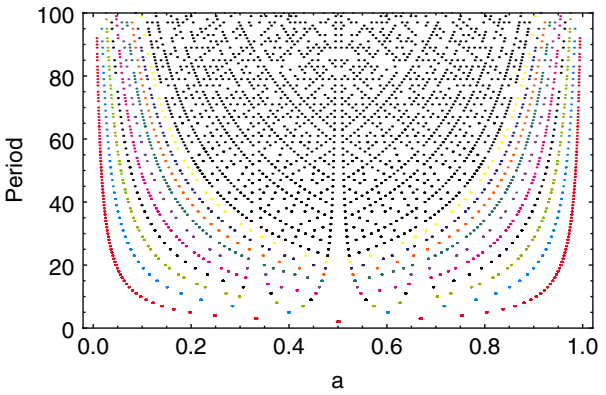

(a)

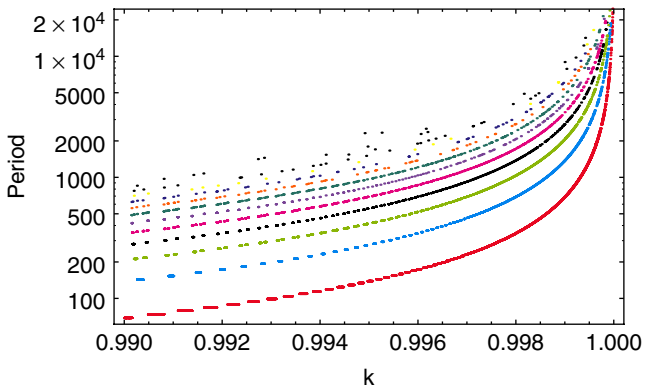

(b)

Fig. 4. Layered structures associated with the Farey sequence. First ten layers are indicated by different colors based on (a) index l and (b) index l'. (a) $k = 0.99$. (b) $a = 0.8$ and $c = 7$.

the Farey sequence. The Farey sequence of order n is a sequence of irreducible fractions $m_1/m_2 \in [0, 1]$, $(m_1,\ m_2 \leq n)$ arranged in ascending order. For example, the Farey sequences of order 1, 2, and 3 are, respectively,

$$F_1 = \left\{\frac{0}{1}, \frac{1}{1}\right\},$$
$$F_2 = \left\{\frac{0}{1}, \frac{1}{2}, \frac{1}{1}\right\}, \tag{8}$$
$$F_3 = \left\{\frac{0}{1}, \frac{1}{3}, \frac{1}{2}, \frac{2}{3}, \frac{1}{1}\right\}.$$

It is known that the devil's staircase pattern with respect to a, as shown in Fig. 3(a), corresponds to the Farey sequence of infinite order [Hata, 1982, 1998]. The denominators of the sequence are the period. The numerators of the sequence are the number of firing events per period, given by

$$f = \sum_{r=1}^{p} u(x^r). \tag{9}$$

The Farey sequence of infinite order contains every possible irreducible fraction within $[0, 1]$. On the other hand, the devil's staircase pattern with respect to k, as shown in Fig. 3(b), may correspond to a part of the Farey sequence of infinite order. This prediction is easily obtained if one considers a continuous transformation of a horizontal section in Fig. 2(a) to a vertical section. The subsequence starts from 1/2 and ends at a certain value that depends on the value of a.

We introduce an index $l = \min(f, p - f)$ to distinguish between the layers in Fig. 4(a). This index can precisely identify the first ten layers in the plot. The envelope of the lth layer is approximately l times higher than that of the bottom layer. This observation can be explained as follows. Consider two parameter values a_1 and a_2 that are very close, i.e. $a_1 \simeq a_2$. Let $\rho_1 = f_1/p_1$ and $\rho_2 = f_2/p_2$ denote the corresponding firing rates. The two firing rates are close, i.e. $\rho_1 \simeq \rho_2$, because the devil's staircase pattern is a continuous function. For simplicity, we assume $\rho_1,\ \rho_2 < 1/2$. Then, we obtain $p_2 \simeq (f_2/f_1)p_1 = (l_2/l_1)p_1$, where l_1 and l_2 are the indexes associated with a_1 and a_2, respectively. In particular, if $l_1 = 1$, we obtain $p_2 \simeq l_2\, p_1$.

The index l cannot capture the layered structure in Fig. 4(b). Thus, we introduce another index $l' = g(c(1 - k)\min(f, p - f))$, where g is the rounding function and c is a scalar value that depends on a. By using this index, we can precisely differentiate between the layers in Fig. 4(b). The relationship between the two indexes l and l' is not clear yet. However, we may be able to integrate them into a unified framework.

The existence of the layered structures indicates that the period of the NS model is sensitive to parameter changes, especially when k is close to 1. In contrast, the firing rate shows a monotonous increase against both a and k, and the transient length does not show such sensitivity.

3. Two Coupled NS Models

The dynamics of two coupled NS models is described as

$$x_1(t + 1) = k\, x_1(t) - y_1(t) + a, \tag{10}$$

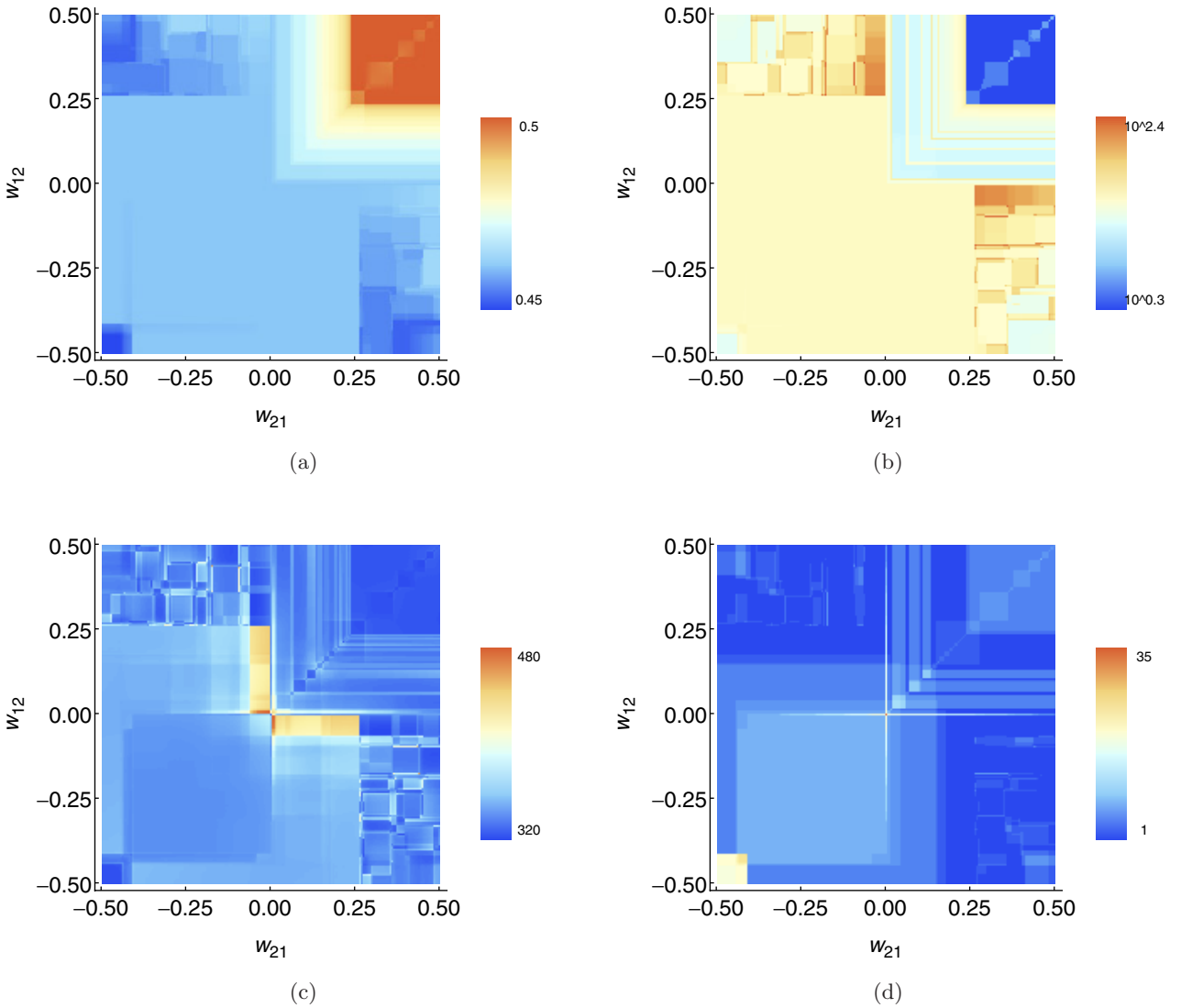

Fig. 5. Phase diagrams of two coupled Nagumo–Sato models with $a = 0.45$ and $k = 0.9$. (a) Average firing rate. (b) Average period. (c) Average transient length. (d) Number of coexisting attractors. The color bar in (b) is scaled logarithmically. Initial states $(x_1(0), x_2(0))$ are taken from 10 000 equally spaced points in $[-1, 1] \times [-1, 1]$, and $y_1(0) = y_2(0) = 0$.

$$x_2(t+1) = k\,x_2(t) - y_2(t) + a, \tag{11}$$

$$y_1(t+1) = u(x_1(t+1) + w_{12}\,y_2(t)), \tag{12}$$

$$y_2(t+1) = u(x_2(t+1) + w_{21}\,y_1(t)), \tag{13}$$

which is a special case of Eqs. (4) and (5).

Figure 5 shows the phase diagrams of the two coupled NS models. In this network system, more than two attractors can coexist for the same parameter configuration. Thus, we determine the average of the statistics over different initial conditions. The average firing rate and the average period show similar structures, as shown in Figs. 5(a) and 5(b). On the other hand, the phase diagram of the average transient length shows a differently structured pattern, as shown in Fig. 5(c). Especially, there are a few discontinuity lines across which the average transient length changes even though neither the average firing rate nor the average period changes (for example, see the line $0.01 < w_{12} < 0.25$ and $w_{21} \simeq -0.06$).

Figure 5(d) shows the number of coexisting attractors. The origin $w_{12} = w_{21} = 0$ has the maximum value 35, which corresponds to the period of an isolated NS model. This is because, without interaction, the two nodes can exhibit phase-locked synchronization with an arbitrary phase shift. The number of attractors tends to be large for $w_{12}, w_{21} < 0$ compared with other regions: $w_{12}, w_{21} > 0$; $w_{12} > 0$, $w_{21} < 0$; and $w_{12} < 0$, $w_{21} > 0$.

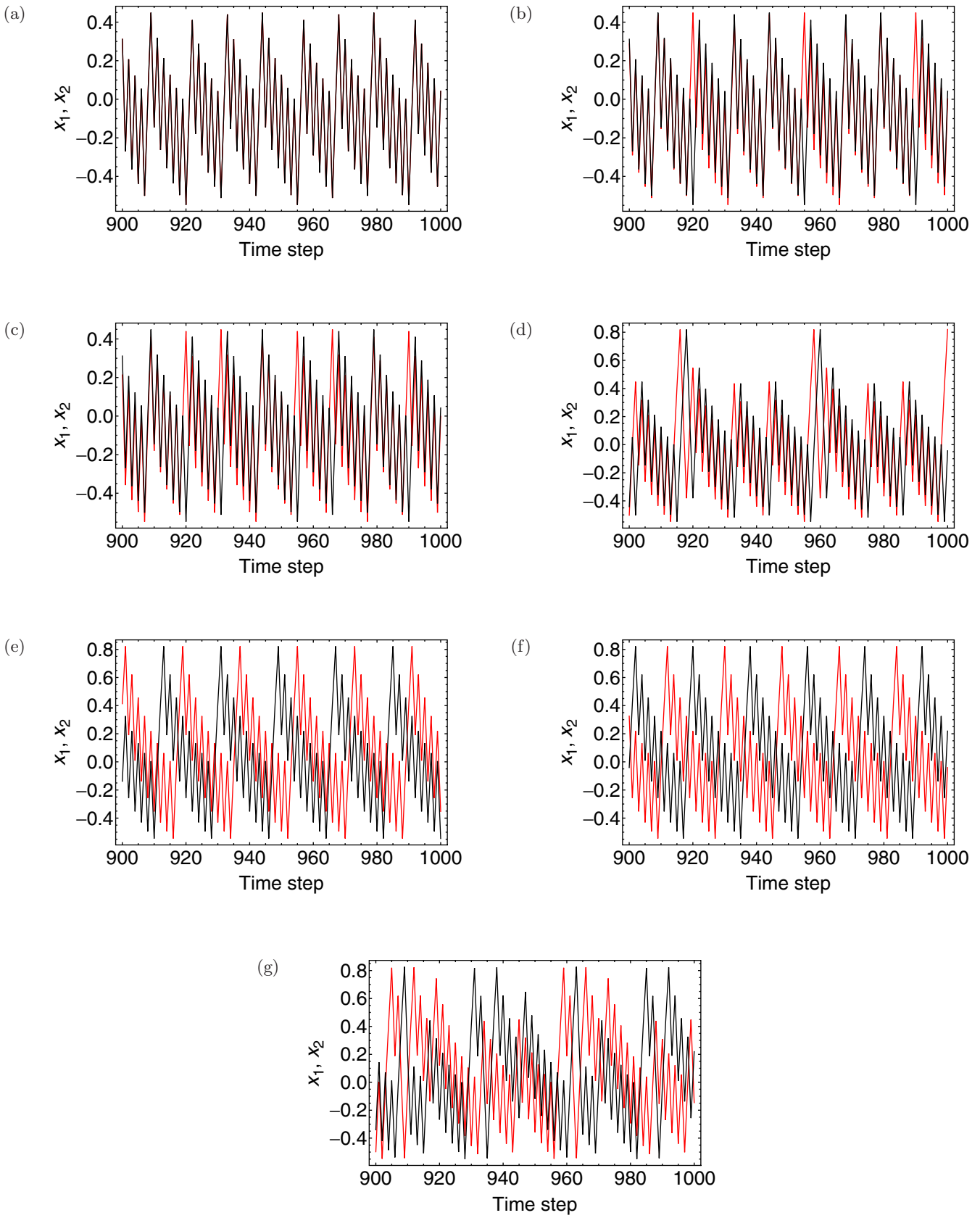

Fig. 6. Examples of coexisting periodic attractors of two coupled Nagumo–Sato models. Black and red lines show the time series of x_1 and x_2, respectively. $a = 0.45$, $k = 0.9$, and $w_{12} = w_{21} = -0.42$.

A part of discontinuity in the average transient length can be attributed to the change in the number of attractors.

The patterns in the phase diagrams, shown in Figs. 5(a)–5(d), continue outside the plotted region. One extreme case of the dynamics outside the plotted region is a fixed-point solution with $\rho = 1$, which exists for very large values of w_{12} and w_{21}.

Figure 6 shows examples of coexisting attractors. Different attractors have different periods and/or different firing rates in general. On the other hand, different attractors sharing the same period and the same firing rate also exist [for example, Figs. 6(a)–6(c)]. To distinguish between different attractors, we introduce an index defined as

$$D = \frac{1}{p}\sum_{r=1}^{p}\frac{x_1^r - x_2^r}{x_1^r + x_2^r}, \tag{14}$$

where $\{(x_1^1, x_2^1), \ldots, (x_1^p, x_2^p)\}$ is a set of periodic points. This quantity shows how the two nodes' states differ on average. It takes 0 if the two nodes are completely synchronized. Otherwise, it takes a nonzero value whose absolute value indicates the level of desynchronization.

Figure 7 shows the basin structure of the coexisting attractors, which is determined by the index D. The parameter values are the same as those of Fig. 6. The fully synchronous solution corresponding to Fig. 6(a) has a basin that includes the diagonal line $x_1(0) = x_2(0)$. The basin of each attractor is fragmented into many small regions, most of which

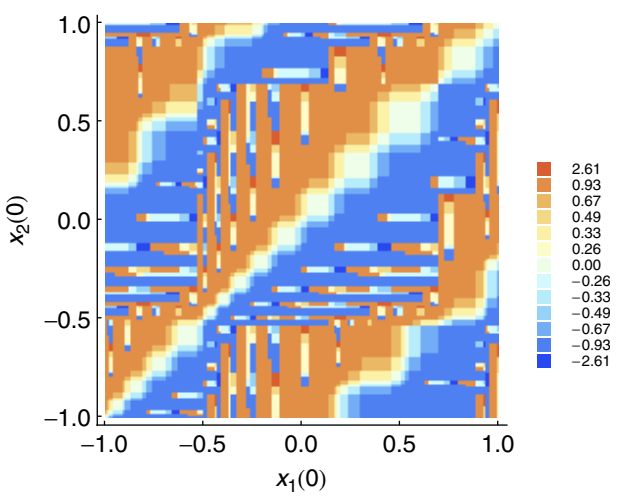

Fig. 7. Basin structure of attractors. Different colors indicate the distinct values of the index D associated with the periodic attractors. The parameter setting is the same as that of Fig. 6. $y_1(0) = y_2(0) = 0$.

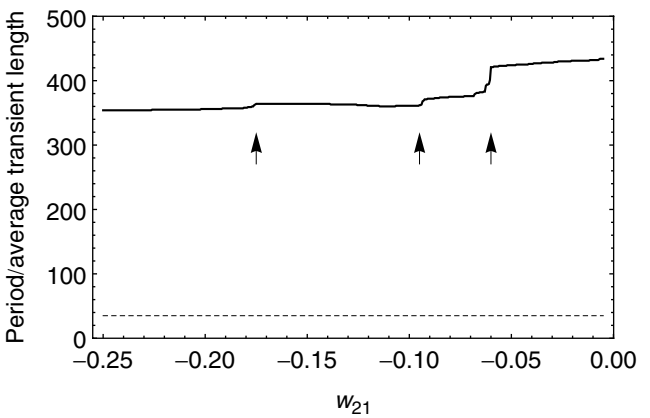

(a)

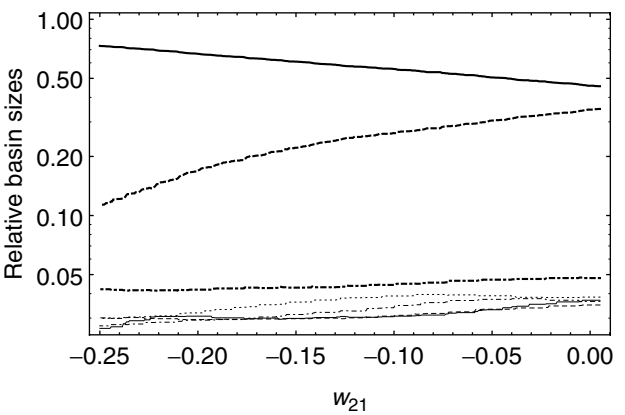

(b)

Fig. 8. (a) Discontinuous changes in the average transient length. The solid line shows the average transient length. The dashed line shows the period that is unique in this parameter range. Arrows indicate the locations of the discontinuous changes. (b) Relative basin sizes of the coexisting attractors. Initial conditions and the parameter values of a and k are the same as those of Fig. 5. $w_{12} = 0.1$.

are rectangular. Neighboring regions tend to have similar values of D.

Figure 8(a) shows a plot of the average transient length that crosses a few discontinuity lines shown in Fig. 5(c). The period is also plotted for reference. Although the transient length has a large variance with respect to the initial states, its mean value exhibits significant changes only when crossing the discontinuity lines. On the other hand, the period does not change at all. In this parameter range, seven attractors coexist. They share the same period and firing rate, and these values are constant. In addition, the basin structure shows only a minor change in the plotted parameter range, and the relative basin sizes of the attractors also cannot explain

the discontinuity, as shown in Fig. 8(b). The discontinuity also appears if we use fixed-point numbers instead of floating-point numbers.

This result is an example of qualitative changes of a dynamical system, which is peculiar to transient dynamics. This type of phenomenon has not been investigated extensively; however, some researchers have reported bifurcation-like phenomena induced by the change of slow parameters [Wang *et al.*, 1994; Johnson *et al.*, 1997; Kang & Tsuda, 2009; Katori *et al.*, 2011]. In addition, Doi *et al.* [1998] reported bifurcations in the second or subsequent eigenvalues of an operator that describe density evolution in a stochastic dynamical system. In the case of the two coupled NS models, more detailed analysis is required to elucidate the mechanism of discontinuous changes in the average transient length.

4. Associative Memory Model Consisting of NS Models

In this section, we investigate an associative memory model that consists of NS models. In general, an associative memory model [Anderson, 1972; Kohonen, 1972; Nakano, 1972; Hopfield, 1982] is an artificial neural network model that has recurrent connections. The model describes how memory patterns are encoded in the network and how they are retrieved through nonlinear dynamics. The memory patterns are binary patterns of length N and are denoted by $\boldsymbol{s}^k = \{s_1^k, \ldots, s_N^k\}$ ($s_i^k \in \{-1, 1\}$, $k = 1, \ldots, K$). Using these binary patterns, we define the weight coefficients of the network as

$$w_{ij} = \frac{\lambda}{K} \sum_{k=1}^{K} s_i^k \, s_j^k, \tag{15}$$

where $\lambda \in \mathbb{R}$ is the weight strength parameter. This equation is integrated into Eqs. (4) and (5), which leads to an associative memory model consisting of NS models.

In this study, we use a set of orthogonal patterns $s_i^k = (-1)^{\lfloor (i-1)/(2^{k-1}) \rfloor}$ ($i = 1, \ldots, N$, $k = 1, \ldots, K$), where $N = 2^K$. For example, if $K = 3$ and $N = 2^K = 8$, the patterns are

$$\begin{aligned} \boldsymbol{s}^1 &= \{1, -1, 1, -1, 1, -1, 1, -1\}, \\ \boldsymbol{s}^2 &= \{1, 1, -1, -1, 1, 1, -1, -1\}, \\ \boldsymbol{s}^3 &= \{1, 1, 1, 1, -1, -1, -1, -1\}. \end{aligned} \tag{16}$$

This type of the orthogonal pattern set [Tsuda, 1992] is related to the Rademacher function $F_{\mathrm{radem}}(x, l) = \mathrm{sgn}(\sin(2^l \pi x))$ ($x \in [0, 1]$) through the equation $s_i^k = F_{\mathrm{radem}}((i - 0.5)/N, K - k + 1)$.

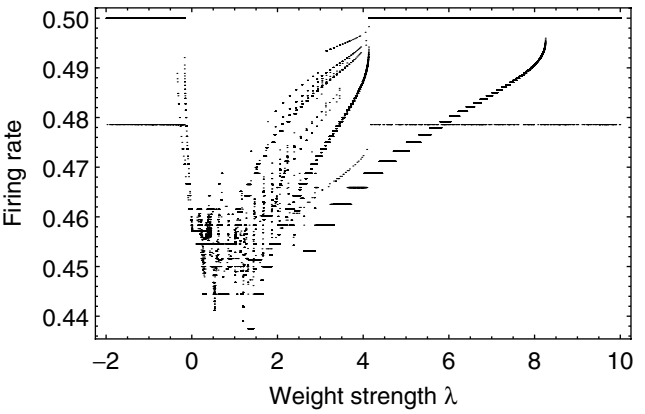

(a)

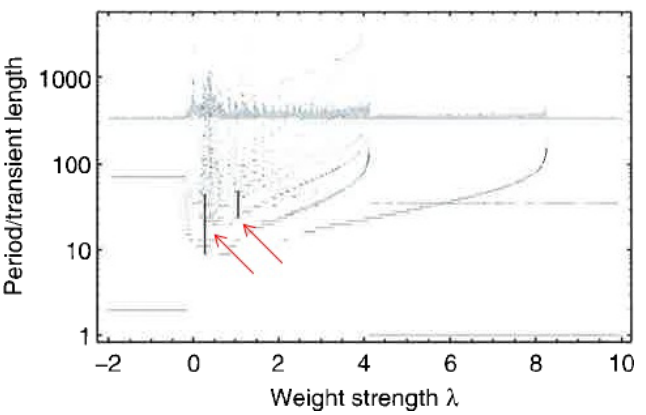

(b)

Fig. 9. Plots of (a) the firing rate and (b) the period and the transient length in an associative memory model consisting of Nagumo–Sato models. Black and blue dots in (b) show the period and the transient length, respectively. Initial states $x_i(0)$ ($i = 0, \ldots, N$) are randomly sampled from the uniform distribution in $[-1, 1]$, and $y_i(0) = 0$. The number of trials is 100. $a = 0.45$, $k = 0.9$, $K = 3$, and $N = 8$.

Figure 9 shows the effect of the weight strength λ on the firing rate, period, and transient length. Both the firing rate and the period exhibit complicated structures characterized by many "staircase" patterns. Some of the staircases form layered structures (for example, $2 < \lambda < 4$) and some exist even for $\lambda < 0$. Interestingly, the period sometimes becomes larger than the transient length. Note that these layers are not necessarily exclusive in the parameter space, as for the case of a single NS model, but some layers coexist.

On the other hand, the transient length does not show staircase patterns, but it changes almost

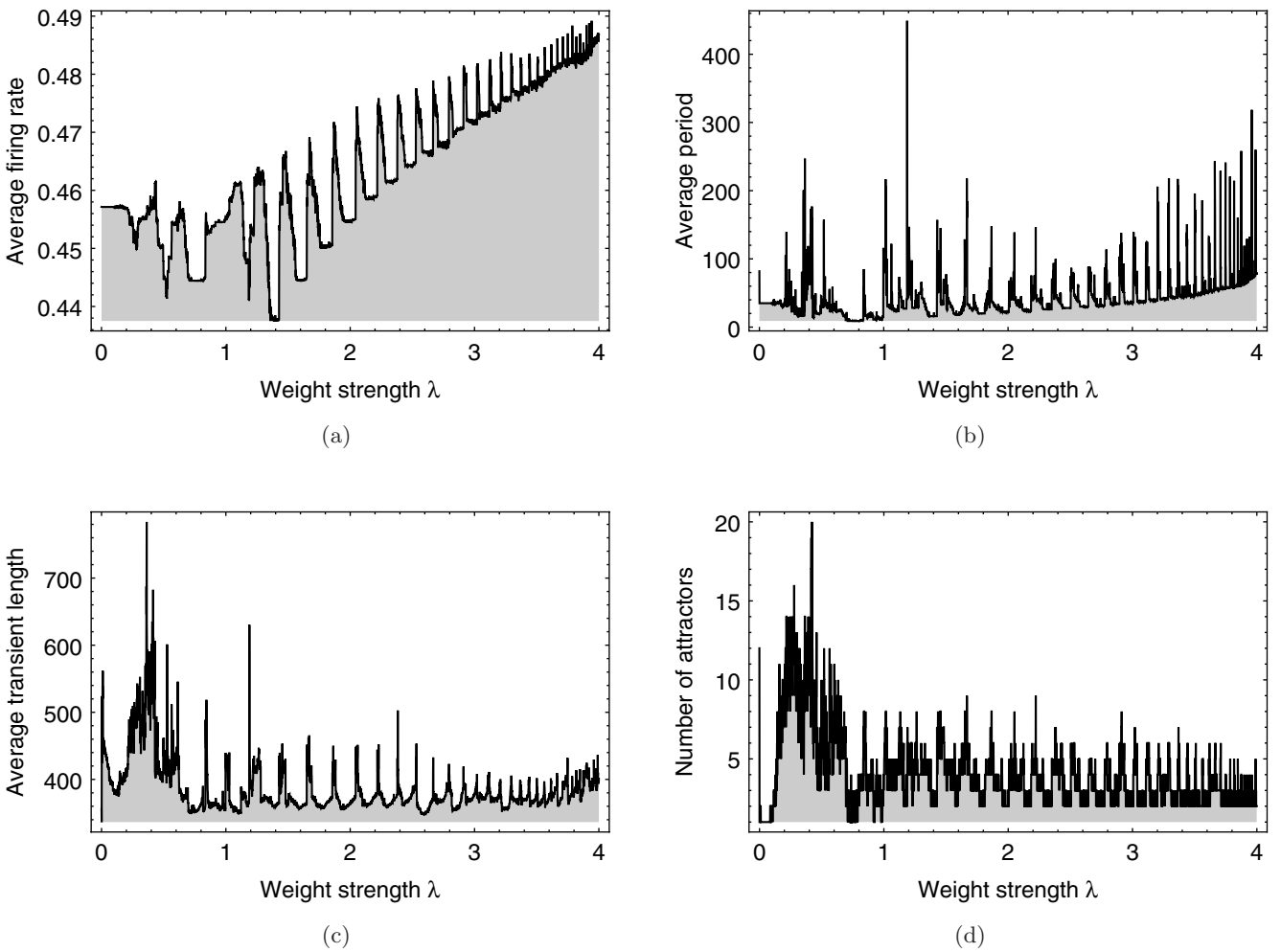

Fig. 10. Oscillations of statistics with respect to the weight strength λ. (a) Average firing rate. (b) Average period. (c) Average transient length. (d) Number of coexisting attractors. Attractors with the same firing rate and period are regarded as identical. The parameter setting is the same as that of Fig. 9.

periodically in a certain parameter range (approximately, $1 < \lambda < 3$). In fact, not only the transient length but also some other statistics show oscillations with respect to λ, as shown in Fig. 10. The average transient length is negatively correlated with the average firing rate and positively correlated with both the average period and the number of attractors. For simplicity, we differentiate attractors only in terms of the firing rate and the period. In fact, many attractors share the same firing rate and period because the network contains symmetry at various levels [Komuro & Aihara, 2001] and many periodic attractors are invariant under certain permutations of variables.

If we increase the number of patterns from $K = 3$ to $K = 4$, the network exhibits staircase patterns similar to the case of $K = 3$, as shown in Fig. 11(a). In this case, both the average period and the average transient length become considerably large at $\lambda \simeq 0.3$, as shown in Figs. 11(b) and 11(c). We call this phenomenon a burst in the period and the transient length. The average period shows a sharp peak, whereas the average transient length becomes high in a relatively wide region. We can also recognize a few smaller peaks both in the average period and in the average transient length; however, the largest peaks are in the bursting region. The burst phenomenon also occurs for larger K.

The dynamics within the burst is complex. Both the firing rate ρ and each unit's state $x_i(t)$ exhibit complicated behavior, as shown in Figs. 12(a)–12(c). The time series of the firing rate is repeated in half the period, but each unit's state differs between the first and second halves of the periodic cycle. In fact, under a certain permutation of

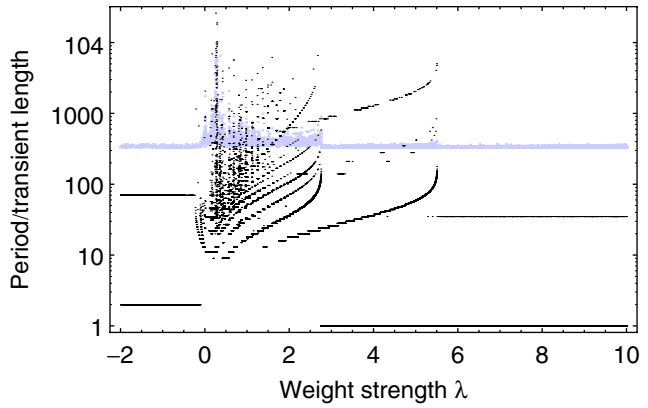

(a)

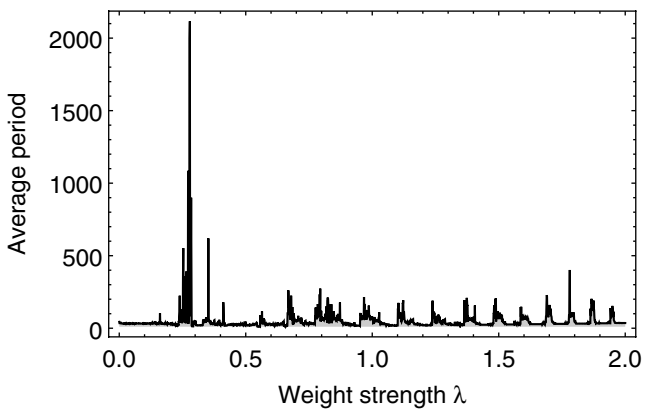

(b)

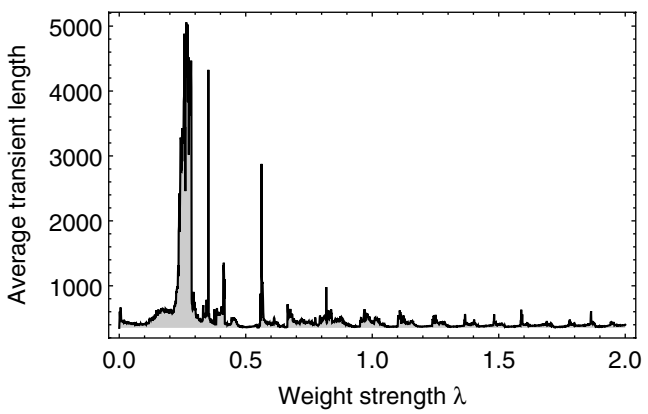

(c)

Fig. 11. Burst in the period and the transient length at $\lambda \simeq 0.3$. (a) Raw values of the period and the transient length. (b) Average period. (c) Average transient length. $a = 0.45$, $k = 0.9$, $K = 4$, and $N = 16$.

variables, the dynamics in the first half completely matches that of the second half.

We also investigate two other statistics, i.e. the quasi-energy $QE(t)$ and the overlap $m^k(t)$, which are important measures for the associative memory model [Adachi & Aihara, 1997]. The quasi-energy is defined as

$$QE(t) = -\frac{1}{2}\sum_{i=1}^{N}\sum_{j=1}^{N} w_{ij}\, y_i(t)\, y_j(t) - \sum_{i=1}^{N} a\, y_i(t). \tag{17}$$

This quantity is low if the network's output is similar to one of the memory patterns. On the other hand, it becomes high if the network's output is random and not similar to any of the patterns. Figure 12(d) shows that the network's output fluctuates between low- and high-energy states both in the transient dynamics and in the periodic cycles. Moreover, the average fluctuation level appears to be different between the transient epoch and the periodic cycles.

Next, the overlap is defined as

$$m^k(t) = 1 - \frac{1}{N}\sum_{i=1}^{N}\left|\frac{s_i^k + 1}{2} - y_i(t)\right|. \tag{18}$$

This quantity shows the overlap of the current network's output with the kth pattern. It is 1 if the network's output completely matches the kth pattern, whereas it is approximately 0.5 for a random output. The value 0 is assigned for the case wherein the network's output matches the reverse pattern of the kth pattern. Figure 12(e) shows that the network visits one of the memory patterns and its reverse pattern in an irregular order in both the transient dynamics and the periodic cycles. On the other hand, there are other memory patterns that are repeatedly visited in the transient dynamics but are never visited in the periodic cycles, as shown in Fig. 12(f).

The reason for the complexity in the long transient dynamics may be partly explained as follows. In the transient epoch, the system's state approaches all the memory patterns. In contract, after the network converges to a periodic orbit, only a part of memory patterns is visited. This means that the network is attracted by many periodic orbits in the transient dynamics, and such attraction probably provides the complexity in the transient dynamics. In addition, the transient length may increase if the coexisting attractors are equally attractive. Indeed, the symmetry in the memory patterns is not a necessary condition of the complex dynamics because nonorthogonal patterns can also result in complex behavior of the network. Nevertheless, the mechanism of the burst is very

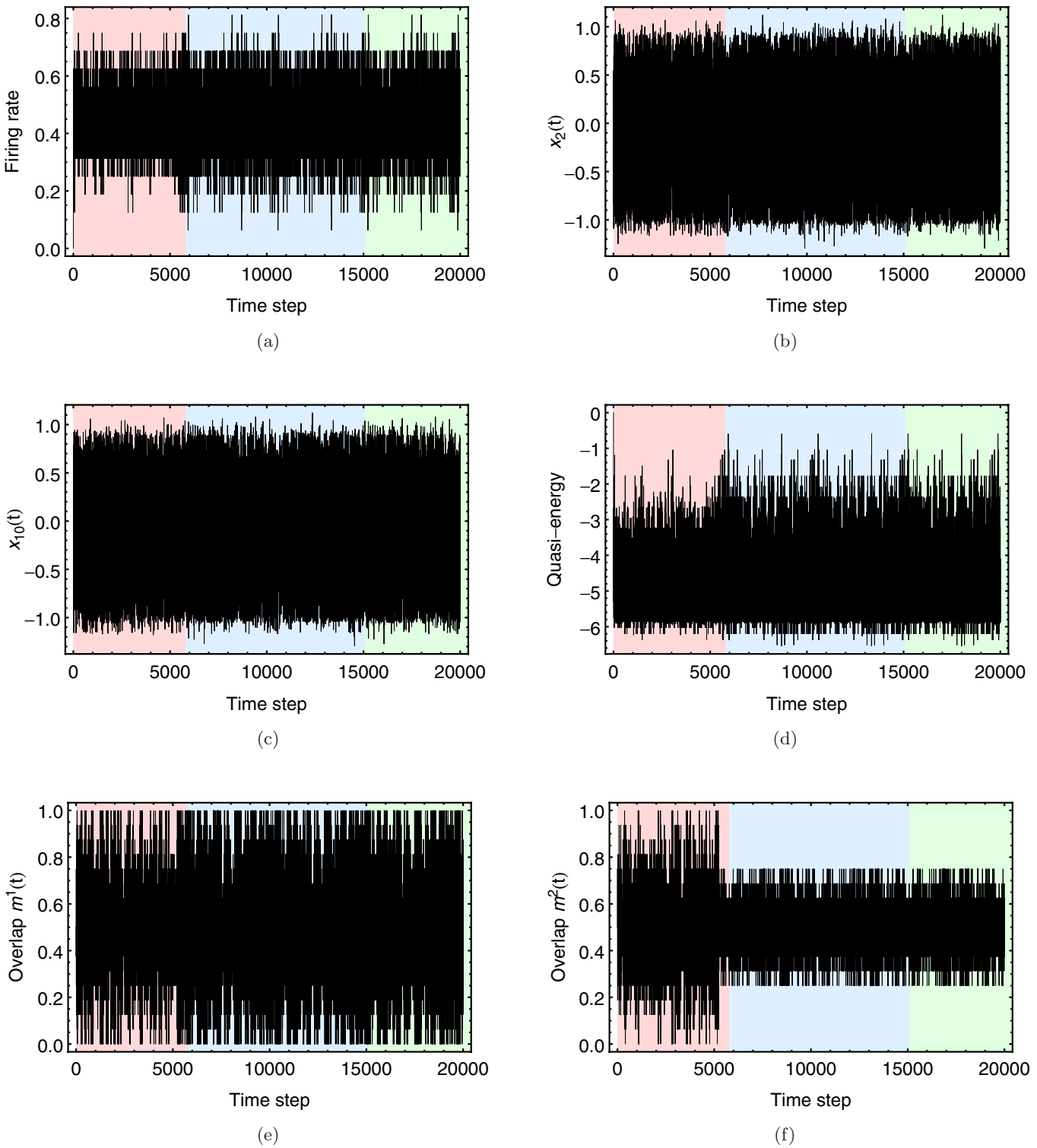

Fig. 12. An example of the dynamics in the burst. (a) Firing rate; (b), (c) single units' states; (d) quasi-energy; (e), (f) overlap between the network's output and memory patterns. Red, blue, and green shadows indicate the transient epoch, the first periodic cycle, and the second periodic cycle, respectively. The parameter setting is the same as that of Fig. 11. $\lambda = 0.279$.

complex and a complete understanding is yet to be achieved.

5. Conclusions

In this study, we have investigated the period and the transient length in single and coupled NS models. The results of numerical simulations indicated the following. First, the period of the single NS model shows layered structures, which are especially apparent when k is close to 1. The layers can be differentiated by the indexes associated with the Farey sequence. Next, the two coupled NS models show discontinuous changes in the transient length, which are not accompanied by any qualitative change in the period, firing rate, or basin structure. Finally, the associative memory model consisting of NS models shows the burst phenomenon, which is characterized by considerably long period and transient length and by complicated dynamics.

As our findings are mainly based on numerical simulations, further analytical consideration is required to clarify the mathematical background. In addition, the findings could improve our understanding of other models such as the chaotic neuron model and the chaotic neural network model [Aihara, 1990; Aihara *et al.*, 1990; Adachi & Aihara, 1997] because the dynamics of the single and coupled NS models may serve as a skeleton of their chaotic dynamics.

Acknowledgments

This research is partially supported by the Japan Society for the Promotion of Science, a Grant-in-Aid for JSPS Fellows (21·937) and the Aihara Project, the FIRST program from JSPS, initiated by CSTP.

References

Adachi, M. & Aihara, K. [1997] "Associative dynamics in a chaotic neural network," *Neural Netw.* **10**, 83–98.

Aihara, K. [1990] "Chaotic neural networks," *Bifurcation Phenomena in Nonlinear Systems and Theory of Dynamical Systems*, ed. Kawakami, H. (World Scientific, Singapore), pp. 143–161.

Aihara, K., Takabe, T. & Toyoda, M. [1990] "Chaotic neural networks," *Phys. Lett. A* **144**, 333–340.

Aihara, K. & Suzuki, H. [2010] "Theory of hybrid dynamical systems and its applications to biological and medical systems," *Phil. Trans. R. Soc. A* **368**, 4893–4914.

Anderson, J. A. [1972] "A simple neural network generating an interactive memory," *Math. Biosci.* **14**, 197–220.

Bak, P. [1986] "The devil's staircase," *Phys. Today* **39**, 38–45.

Bockman, S. [1991] "On-off, discrete-time control of a stable first-order linear plant," *Proc. ACC'91* (IEEE), pp. 1258–1262.

Caianiello, E. R. [1961] "Outline of a theory of thought-processes and thinking machines," *J. Theor. Biol.* **1**, 204–235.

Crutchfield, J. & Kaneko, K. [1988] "Are attractors relevant to turbulence?" *Phys. Rev. Lett.* **60**, 2715–2718.

Ding, E. & Hemmer, P. [1987] "Exact treatment of mode locking for a piecewise linear map," *J. Stat. Phys.* **46**, 99–110.

Doi, S., Inoue, J. & Kumagai, S. [1998] "Spectral analysis of stochastic phase lockings and stochastic bifurcations in the sinusoidally forced van der Pol oscillator with additive noise," *J. Stat. Phys.* **90**, 1107–1127.

Harmon, L. D. [1961] "Studies with artificial neurons. I. Properties and functions of an artificial neuron," *Kybernetik* **1**, 89–101.

Hata, M. [1982] "Dynamics of Caianiello's equation," *J. Math. Kyoto Univ.* **22**, 155–173.

Hata, M. [1998] *Chaos in Neural Network Models* (in Japanese), (Asakura Shoten, Tokyo).

Hopfield, J. J. [1982] "Neural networks and physical systems with emergent collective computational abilities," *Proc. Natl. Acad. Sci. USA* **79**, 2554–2558.

Johnson, B. R., Scott, S. K. & Thompson, B. W. [1997] "Modelling complex transient oscillations for the BZ reaction in a batch reactor," *Chaos* **7**, 350–358.

Kaneko, K. [1985] "Spatiotemporal intermittency in coupled map lattices," *Prog. Theor. Phys.* **74**, 1033–1044.

Kaneko, K. [1990] "Supertransients, spatiotemporal intermittency and stability of fully developed spatiotemporal chaos," *Phys. Lett. A* **149**, 105–112.

Kang, H. & Tsuda, I. [2009] "On embedded bifurcation structure in some discretized vector fields," *Chaos* **19**, 033132.

Katori, Y., Sakamoto, K., Saito, N., Tanji, J., Mushiake, H. & Aihara, K. [2011] "Representational switching by dynamical reorganization of attractor structure in a network model of the prefrontal cortex," *PLoS Comput. Biol.* **7**, e1002266.

Kinoshita, K., Ueta, T., Imura, J. & Aihara, K. [2010] "Bifurcation analysis of coupled Nagumo–Sato models," *Proc. NOLTA'10*, pp. 488–491.

Kohonen, T. [1972] "Correlation matrix memories," *IEEE Trans. Comput.* **c-21**, 353–359.

Komuro, M. & Aihara, K. [2001] "Hierarchical structure among invariant subspaces of chaotic neural networks," *Japan J. Indust. Appl. Math.* **18**, 335–357.

Nagumo, J. & Sato, S. [1972] "On a response characteristic of a mathematical neuron model," *Kybernetik* **10**, 155–164.

Nakano, K. [1972] "Associatron — A model of associative memory," *IEEE Trans. Syst. Man Cybern.* **2**, 380–388.

Politi, A., Livi, R., Oppo, G. & Kapral, R. [1993] "Unpredictable behaviour in stable systems," *Europhys. Lett.* **22**, 571–576.

Tomita, K. & Tsuda, I. [1980] "Towards the interpretation of Hudson's experiment on the Belousov–Zhabotinsky reaction," *Prog. Theor. Phys.* **64**, 1138–1160.

Tsuda, I. [1981] "Self-similarity in the Belousov–Zhabotinsky reaction," *Phys. Lett. A* **85**, 4–8.

Tsuda, I. [1992] "Dynamic link of memory — Chaotic memory map in nonequilibrium neural networks," *Neural Netw.* **5**, 313–326.

Wang, J., Sørensen, P. G. & Hynne, F. [1994] "Transient period doublings, torus oscillations, and chaos in a closed chemical system," *J. Phys. Chem.* **98**, 725–727.

Appendix

In this section, we explain our method for calculating the period p and the transient length τ. The simplest approach is to use a database for the registration of the time series $\{X(0), X(1), \ldots\}$. Then, in each time step t, we check whether any recurrence $X(t) = X(s)$ $(0 \le s \le t-1)$ occurs. The first detection of a recurrence gives both p and τ. However, this simple method requires a memory size of $\mathrm{O}(p+\tau)$, and the computational cost for the recurrence check is also large (for example, $\mathrm{O}(\log(p+\tau)!)$ in the case of a binary search method).

As the single and coupled NS models occasionally have large p and τ, we use the following method instead, which does not require the exhaustive recurrence check. This method consists of two parts (see Table 1). The first part is devoted to calculating only the period p. In this part, we do not require to remember every past state. Instead, we maintain only one reference state in the past sequence and update it intermittently. Specifically, we use a set of reference time steps $t_{\mathrm{ref}}^{(n)}$ $(n = 0, 1, \ldots)$, at which the reference state is updated. The reference state is denoted by $X_{\mathrm{ref}}^{(n)} = X(t_{\mathrm{ref}}^{(n)})$. The reference time steps are calculated as $t_{\mathrm{ref}}^{(0)} = 0$ and $t_{\mathrm{ref}}^{(n+1)} = t_{\mathrm{ref}}^{(n)} + 2^n$. In each time step, the current state $X(t)$ is compared with the latest reference state $X_{\mathrm{ref}}^{(n)}$, which is updated every time we pass through a new reference time step. The first detection event of a recurrence gives the period p. At that moment, the latest reference state is on the periodic orbit and the interval between the current and the next reference time steps is larger than p.

In the second part, the transient length τ is calculated. We compute again the time evolution of the system in two runs $X(t)$ and $X'(t+p)$. In each time step, we update each run for one step and compare the two states. When the two runs share the same value for the first time, we obtain the transient length τ. The time series of $X(t)$ can be obtained from that of $X'(t+p)$ if the latest p steps of $X'(t+p)$ are maintained in the computer memory.

Table 1. Algorithms for the calculation of the period and the transient length.

Calculation of the Period p
$n \leftarrow 0$
$X_{\mathrm{ref}}^{(0)} \leftarrow X(0)$
for $t = 0, 1, \ldots$
$\quad X(t+1) \leftarrow F(X(t))$
$\quad$ **if** $X(t+1) = X_{\mathrm{ref}}^{(n)}$ **then**
$\quad\quad p \leftarrow t + 1 - t_{\mathrm{ref}}^{(n)}$
$\quad\quad$ **break**
$\quad$ **end if**
$\quad$ **if** $t+1 = t_{\mathrm{ref}}^{(n+1)}$ **then**
$\quad\quad X_{\mathrm{ref}}^{(n+1)} \leftarrow X(t+1)$
$\quad\quad n \leftarrow n+1$
$\quad$ **end if**
end for

Calculation of the Transient Length τ
$X'(0) \leftarrow X(0)$
for $t = 0, 1, \ldots, p-1$
$\quad X'(t+1) \leftarrow F(X'(t))$
end for
for $t = 0, 1, \ldots$
$\quad$ **if** $X(t) = X'(t+p)$ **then**
$\quad\quad \tau \leftarrow t$
$\quad\quad$ **break**
$\quad$ **end if**
$\quad X(t+1) \leftarrow F(X(t))$
$\quad X'(t+p+1) \leftarrow F(X'(t+p))$
end for